Chinese Chemical Letters 35 (2024) 108549

Contents lists available at ScienceDirect

Chinese Chemical Letters

journal homepage: www.elsevier.com/locate/cclet

One-step conversion of methane and formaldehyde to ethanol over SA-FLP dual-active-site catalysts: A DFT study

Tao Ban[a], Xi-Yang Yu[a], Hai-Kuo Tian[a], Zheng-Qing Huang[a], Chun-Ran Chang[a,b,*]

[a] Shaanxi Key Laboratory of Energy Chemical Process Intensification, School of Chemical Engineering and Technology, Xi'an Jiaotong University, Xi'an 710049, China

[b] Shaanxi Key Laboratory of Low Metamorphic Coal Clean Utilization, School of Chemistry and Chemical Engineering, Yulin University, Yulin 719000, China

ARTICLE INFO

Article history:
Received 12 April 2023
Revised 25 April 2023
Accepted 8 May 2023
Available online 9 May 2023

Keywords:
Single-atom
Frustrated Lewis pairs
Methane conversion
Dual active sites
Ethanol synthesis

ABSTRACT

One-step conversion of methane and formaldehyde into ethanol is a 100% atom-efficient process for carbon resources utilization and environment protection but still faces eminent challenges due to the lacking of efficient catalysts. Therefore, developing active and stable catalysts is crucial for the co-conversion of methane and formaldehyde. Herein, twelve kinds of "Single-Atom" - "Frustrated Lewis Pair" (SA-FLP) dual-active-site catalysts are designed for the direct conversion of methane and formaldehyde to ethanol based on density functional theory (DFT) calculations and microkinetic simulations. The results show that the SA-FLP dual active sites can simultaneously activate methane at the SA site and activate formaldehyde at the FLP site. Among the twelve designed SA-FLP catalysts, Fe_1-FLP shows the best performance in the co-conversion of methane and formaldehyde to ethanol with the rate-determining barrier of 1.15 eV. Ethanol is proved as the main product with the turnover frequency of 1.32×10^{-4} s^{-1} at 573 K and 3 bar. This work provides a universal strategy to design dual active sites on metal oxide materials and offers new insights into the effective conversion of methane and formaldehyde to desired C_2 chemicals.

Methane (CH_4), the major component of natural gas and a key constituent of greenhouse gases, is usually taken as an important chemical feedstock to produce value-added chemicals [1–3]. Formaldehyde (HCHO), the dominant pollutant of the indoor air, is also widely used as feedstock in many industrial processes [4–6]. Particularly, the use of CH_4 and HCHO as raw materials to produce high value-added chemicals would be very attractive. Ethanol (CH_3CH_2OH), an ideal product from the conversion of CH_4 and HCHO, plays an important role in the food processing and organic chemical industry [7–9]. The direct conversion of CH_4 and HCHO into CH_3CH_2OH is appealing for two reasons. First, this reaction is a green and 100% atom-efficient process, which can reduce the implementation steps. Second, the catalytic reaction of CH_4 and HCHO to synthesize CH_3CH_2OH with high utilization value is of great significance in environmental protection and sustainable development [10,11]. However, there are few studies on the direct conversion of CH_4 and HCHO to CH_3CH_2OH due to the lacking of efficient catalysts. Therefore, the development of practical and high-performance catalysts for synthesizing CH_3CH_2OH from CH_4 and HCHO is extremely urgent.

Currently, the catalytic materials used in CH_4 and HCHO activation are mainly oxide-supported transition metal (TM/oxide) catalysts [11–15]. For instance, the most popular catalysts used for the oxidation of HCHO into harmless gases are Pt/oxide catalysts, such as Pt/TiO_2, Pt/MnO_2, and Pt/Fe_2O_3 [16–18]. In addition, Al_2O_3-, ZrO_2- and CeO_2-supported Au and Ag catalysts have also been found to be active for the HCHO oxidation [19–22]. On the other hand, TM/oxide catalysts were also extensively used in the methane activation such as Pt/Ga_2O_3, Fe/V_2O_3, and Pd/CeO_2 [23–27]. Thus, the one-step conversion of CH_4 and HCHO to ethanol at TM/oxide is still of great promise. Among these TM/oxides, CeO_2 as support have gained much attention due to its outstanding capacities to release and store oxygen atoms [28–31] and the ability to stabilize transition metals with high dispersion [32–36]. However, the TM/CeO_2 catalysts are difficult to simultaneously activate CH_4 and HCHO due to the surface adsorption competition between the two molecules. Therefore, the design of dual-active-site catalysts that can selectively and simultaneously activate CH_4 and HCHO is of great demand for the effective conversion of the two compounds. Recently, we have proposed a new strategy to construct single-atom and frustrated-Lewis-pair (SA-FLP) dual active sites *via*

* Corresponding author at: Shaanxi Key Laboratory of Energy Chemical Process Intensification, School of Chemical Engineering and Technology, Xi'an Jiaotong University, Xi'an 710049, China.
E-mail address: changcr@mail.xjtu.edu.cn (C.-R. Chang).

https://doi.org/10.1016/j.cclet.2023.108549
1001-8417/

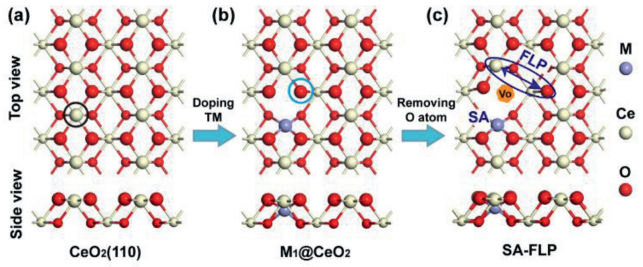

Fig. 1. Top and side view of the optimized of (a) $CeO_2(110)$, (b) $M_1@CeO_2$, and (c) SA-FLP. The black circle in (a) represents the position where the Ce atom is replaced by TM atoms, and the blue circle in (b) represents the position where the O atom is removed.

TM-doping and surface oxygen vacancies regulating on CeO_2 surfaces [37,38]. We found that the doped TM single-atom into CeO_2 could serve as an active site to activate CH_4. At the same time, the FLP site created by removing neighboring oxygen atoms around TM atoms, can serve as another active site for the activation of other small molecules, such as CO_2 [37], CH_4 [38] and H_2O [39]. Therefore, inspired by previous studies, SA-FLP dual-active-site catalysts are also expected to have unique catalytic behaviors in the activation and conversion of CH_4 and HCHO into ethanol.

In this work, SA-FLP dual active sites are constructed by doping the TM atoms (TM = Fe, Co, Ni, Cu; Ru, Rh, Pd, Ag; Os, Ir, Pt, Au) into $CeO_2(110)$ surface and regulating the surface oxygen vacancies. Upon the designed SA-FLP dual active sites, the adsorption/activation behavior of CH_4 and HCHO are explored at SA and FLP sites, respectively. The spatial proximity of the dual active sites enables the C−C coupling of CH_4 and HCHO to C_2 products. The reaction mechanism of the co-conversion of CH_4 and HCHO to C_2 products are comprehensively studied by density functional theory (DFT) calculations and microkinetic modeling. The computational details can be found in the Supporting information. This work provides insights into the development of dual active sites on metal oxide catalysts for the effective conversion of CH_4 and HCHO to desired C_2 chemicals.

Our previous studies have indicated that SA-FLP dual active sites can be successfully constructed at the $CeO_2(110)$ surface [37,38]. As shown in Fig. 1a, the SA sites are constructed by doping TM atoms at the Ce sites of $CeO_2(110)$ surface. The FLP sites are created by removing the most unstable surface oxygen atom neighboring to TM atoms (Fig. 1b), resulting in the unbonded Ce···O pairs as the FLP sites (Fig. 1c). In the present work, the TMs, including Fe, Co, Ni, Cu, Ru, Rh, Pd, Ag, Os, Ir, Pt, and Au are selected to construct the SA site on the $p(2 \times 3)$ $CeO_2(110)$ surface (Fig. S1 in Supporting information). The FLP sites are fabricated by removing the second neighboring surface oxygen atom (the most unstable one) of the TM atoms (Fig. S2 in Supporting information). The constructed SA-FLP dual active sites have a distance of ~4 Å (Fig. 1c), paving the way for the simultaneous activation of two small molecules.

Upon the designed SA-FLP dual active sites, the adsorption behavior of HCHO was explored at SA and FLP sites, respectively. As shown in Fig. 2a, the calculated adsorption energies of the HCHO molecule at the SA sites range from –0.60 eV (Au_1-FLP) to –0.21 eV (Ir_1-FLP). While the values at FLP sites range from –1.04 eV (Au_1-FLP) to –0.44 eV (Co_1-FLP), which are much higher (in absolute value) than those on SA sites, indicating the adsorption of HCHO at the FLP site is more favorable than that at SA site. The difference in adsorption energies is mainly due to the different adsorption configurations of HCHO at the SA and FLP sites. On SA sites, the HCHO molecule is tilted to the SA site with its two H atoms pointing to the SA sites (Fig. S3 in Supporting information), meanwhile, the C–O bond lengths are elongated from 1.214 Å to approximately 1.220 Å and two C–H bond length are changed from 1.118 Å to approximately 1.115 and 1.120 Å, respectively (Table S1 in Supporting information). Whereas on FLP sites, the HCHO molecule is vertically adsorbed with its O and H atoms adsorbed at the acidic and base sites, respectively (Fig. S4 in Supporting information). The C–O bond lengths are elongated from the gas-phase 1.214 Å to approximately 1.228 Å, which is longer than that on the SA site (~1.220 Å) (Table S1 in Supporting information). These results indicate that the HCHO molecule prefers to adsorb at FLP sites. Therefore, the adsorption/activation of HCHO molecules at the FLP site was selected in the following study.

As we have previously reported, CH_4 prefers to be adsorbed at SA sites rather than at FLP sites on the SA-FLP catalysts [37]. Therefore, in the present study the dissociative activation of CH_4 at SA sites is also adopted, which follows two different routes. One starts with CH_4 adsorption/activation followed by the HCHO adsorption (denoted as route-1, Fig. S5a in Supporting information), and another starts with the HCHO adsorption followed by the CH_4 adsorption/activation (denoted as route-2, Fig. S5b in Supporting information). The adsorption energies, reaction energies, and activation energies of CH_4 at different routes are given in Figs. 2b–d, and the adsorption energies of HCHO at different routes are depicted in Fig. S6 (Supporting information). One can see that CH_4 has larger adsorption energies (in absolute value) on route-1 than that on route-2 over most of the SA-FLP catalysts except Co_1-FLP, Os_1-FLP, and Ir_1-FLP, indicating that the pre-adsorbed HCHO molecules hinder the adsorption of methane on the surface (Fig. 2b). Similar to the adsorption of methane, in most cases the adsorption of HCHO is also enhanced with the pre-adsorbed methane (Fig. S6 in Supporting information). Upon the two adsorption configurations, CH_4 undergoes heterolytically dissociation at the SA site, where the methyl group is anchored at the SA site and the H atom is adsorbed at the adjacent O site. Comparing the two routes, the dissociative activation of CH_4 in route-1 is thermodynamically and kinetically more favorable, as shown by the corresponding reaction energies and activation barriers (Figs. 2c and d). Thus, the route-1, *i.e.*, CH_4 adsorption/activation first followed by HCHO adsorption/activation, is more preferential to occur and thus is selected for further study.

After the co-activation of CH_4 and HCHO, the activated CH_3^* and HCHO* are adsorbed on the SA site and the FLP site, respectively. In this section, the co-conversion of CH_4 and HCHO to ethanol over the twelve kinds of SA-FLP catalysts is further explored. The reaction pathways consisting of seven steps are as follows: (i, ii) the adsorption/activation of CH_4 at the SA site (state 1–3 in Fig. S7 in Supporting information, R1–2 in Table S2 in Supporting information), (iii) the adsorption/activation of HCHO at FLP site (state 3–4 in Fig. S7, R3 in Table S2), (iv) the C–C coupling of CH_3^* and HCHO* to $CH_3CH_2O^*$ intermediate (state 4–5 in Fig. S7, R4 in Table S2), (v, vi) the migration of H atom from Lewis base site (O atom) to $CH_3CH_2O^*$ intermediate to form ethanol (state 5–7 in Fig. S7, R5–6 in Table S2), (vii) the desorption of ethanol (state 7–8 in Fig. S7, R7 in Table S2). The values of reaction energy and activation energy are listed in Table 1.

As shown in Table 1, in the first three steps, CH_4 and HCHO are activated to CH_3^* and HCHO*, respectively (R1–3). Among the twelve kinds of SA-FLP catalysts, Co_1-FLP shows the best performance in the adsorption of HCHO with adsorption energy of −1.04 eV, while Os_1-FLP shows the best performance in the dissociative activation of CH_4 with an activation energy of 0.44 eV. The presence of the two groups on the surface increases the possibility of C−C coupling to generate C_2 products. It can be seen that the C–C coupling of CH_3^* and HCHO* to $CH_3CH_2O^*$ intermediate (R4) on all the SA-FLP catalysts are exothermic by –2.61 eV to –0.96 eV, and the corresponding energy barrier varies from 0.09 eV

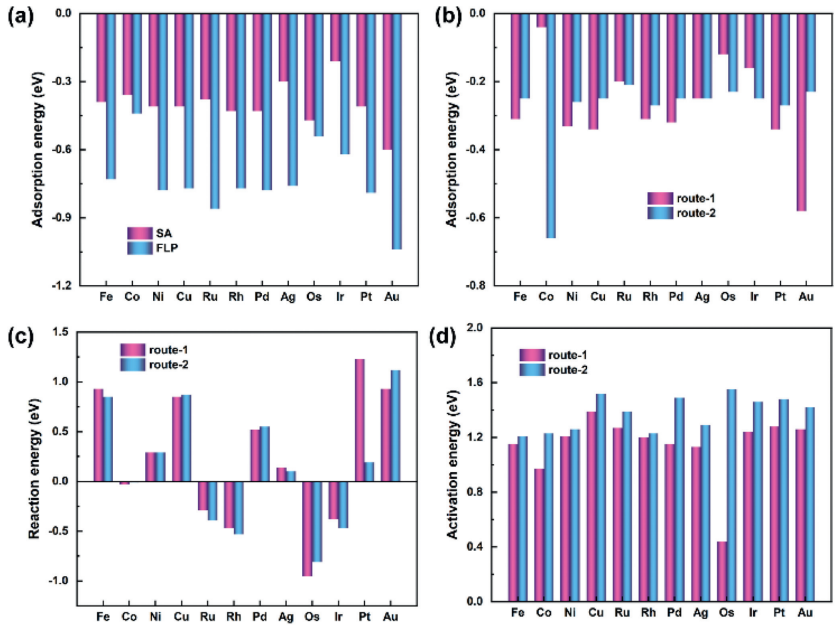

Fig. 2. (a) The adsorption energies of HCHO at different sites. (b) The adsorption energies of CH_4 at different routes. (c) The reaction energies of CH_4 dissociation at different routes. (d) The activation energies of CH_4 dissociation at different routes.

Table 1
The reaction energies and activation energies of the reaction of CH_4 and HCHO to ethanol.

Catalysts	R1	R2		>R3	R4		R5		>R6	>R7
	E_{ads} (eV)	ΔE (eV)	E_a (eV)	E_{ads} (eV)	ΔE (eV)	E_a (eV)	ΔE (eV)	E_a (eV)	ΔE (eV)	ΔE (eV)
Fe_1-FLP	−0.31	0.93	1.15	−0.75	−2.41	0.18	0.72	0.84	0.01	1.10
Co_1-FLP	−0.04	−0.03	0.97	−1.04	−1.48	0.39	0.67	0.78	−0.10	1.31
Ni_1-FLP	−0.33	0.29	1.21	−0.71	−1.82	0.22	0.65	0.79	0.01	1.20
Cu_1-FLP	−0.34	0.85	1.39	−0.66	−2.32	0.18	0.67	0.78	−0.01	1.10
Ru_1-FLP	−0.20	−0.29	1.27	−0.97	−1.17	0.62	0.69	0.84	−0.05	1.28
Rh_1-FLP	−0.31	−0.47	1.20	−0.79	−0.96	0.67	0.64	0.82	−0.02	1.20
Pd_1-FLP	−0.32	0.52	1.15	−0.68	−2.06	0.17	0.64	0.80	−0.01	1.20
Ag_1-FLP	−0.25	0.14	1.13	−0.80	−1.58	0.09	0.65	0.77	−0.07	1.20
Os_1-FLP	−0.12	−0.95	0.44	−0.51	−1.18	0.74	−0.13	0.19	−0.14	2.32
Ir_1-FLP	−0.16	−0.38	1.24	−0.80	−1.10	0.61	0.62	0.66	−0.01	1.07
Pt_1-FLP	−0.34	1.23	1.28	−0.98	−1.71	0.39	0.64	0.82	0.01	1.22
Au_1-FLP	−0.58	0.93	1.26	−0.50	−2.61	0.39	0.63	0.78	−0.04	1.46

to 0.74 eV, indicating that the C−C coupling steps is both thermodynamically and kinetically favorable on all the SA-FLP catalysts. In the subsequent migration of the H proton from the Lewis base site (O atom) to $CH_3CH_2O^*$ intermediate to form ethanol steps (R5–6), Os_1-FLP shows the lowest activation energy (0.19 eV), much lower than that on most of the SA-FLP catalysts (~0.80 eV). However, the ethanol desorption on Os_1-FLP is the most difficult (2.32 eV) compared to the other SA-FLP catalysts (~1.20 eV) (R7). Overall, the rate-determining steps (RDS) of the whole reaction pathway for forming ethanol on the twelve SA-FLP catalysts are different. For most of the SA-FLP catalysts, the RDS is the desorption of ethanol, including Co_1-FLP, Ru_1-FLP, Rh_1-FLP, Pd_1-FLP, Ag_1-FLP, Os_1-FLP, and Au_1-FLP. While the RDS for the other SA-FLP catalysts is the dissociative activation of CH_4. Among the twelve kinds of SA-FLP catalysts, Fe_1-FLP delivers the lowest RDS barrier (1.15 eV), suggesting that Fe_1-FLP is the best candidate for the conversion of CH_4 and HCHO to ethanol and thus is selected for further study. In addition, ab initio molecular dynamics (AIMD) simulations were performed to investigate the stability of the Fe_1-FLP catalyst, which shows that Fe_1-FLP is stable at high temperatures (Fig. S8 in Supporting information).

The possibility of the co-conversion of CH_4 and HCHO to ethylene is also explored based on Fe_1-FLP. As shown in Fig. 3a, in the first four steps, the formation of ethanol (denoted as route-1) and ethylene (denoted as route-2) undergo the same process (A1→ A5). The difference between the two routes is at the beginning of step A5, where route-1 is the migration of the H atom from the Lewis base site (O atom) to $CH_3CH_2O^*$ intermediate (A5→ A6), while route-2 is the conversion of $CH_3CH_2O^*$ intermediate to $CH_2CH_2OH^*$ intermediate (A5→ A9). In comparison of the RDS of the two routes, route-1 (1.15 eV) is much lower than route-2 (2.55 eV), that is, the formation of ethanol is more facile than the formation of ethylene, and thus ethanol remains the main product of the reaction on the designed SA-FLP catalysts.

To explore the feasibility of the reaction under realistic conditions, microkinetic simulations with mean-field approximation were calculated using the CatMAP code [40]. All the elementary reactions in Fig. 3 were considered (Table S2 in Supporting information), and the corresponding structural and formation energy details can be found in Table S3 (Supporting information). The formation energies were calculated using electronic energies of CH_4, H_2, H_2O, and SA-FLP as references. The methane consumption rate and the main product production rate as a function of reaction temperature and pressure are shown in Fig. 4.

It can be seen that the methane consumption rate increases slightly with increasing temperature at a fixed pressure and in-

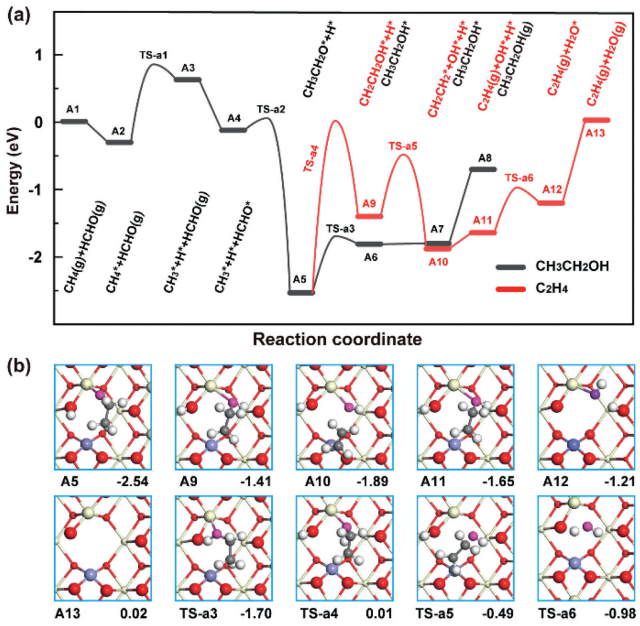

Fig. 3. (a) Potential energy diagram for the reaction of CH_4 and HCHO to ethanol on Fe_1-FLP. The zero energy reference corresponds to the sum of the energies of CH_4(g), HCHO(g), and Fe_1-FLP surface. (b) Corresponding optimized structures of the intermediates and the transition states.

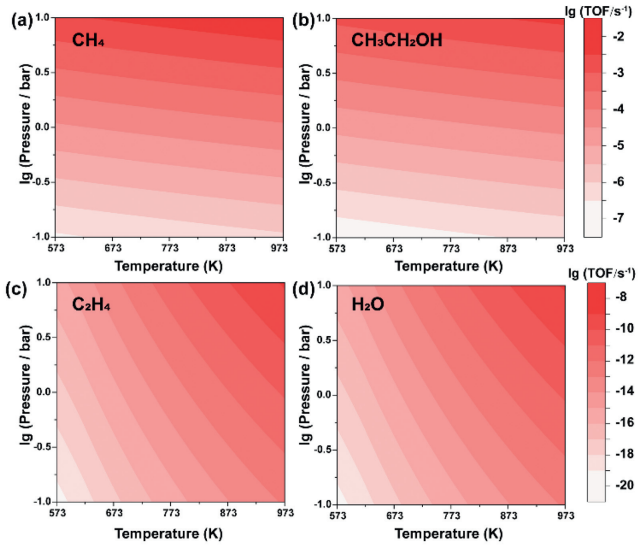

Fig. 4. (a) Turnover frequencies for CH_4 consumption as the function of reaction temperature and the pressure for Fe_1-FLP; Turnover frequencies for (b) CH_3CH_2OH, (c) C_2H_4, and (d) H_2O production as the function of reaction temperature and the pressure for Fe_1-FLP. The initial CH_4/HCHO ratio is 1:1.

creases obviously with increasing pressure at a fixed temperature (Fig. 4a), suggesting that the high methane consumption rate can be achieved at reaction conditions of high temperature and high pressure. At the temperature of 573 K and the pressure of 1 bar, the TOF of CH_4 consumption is 2.64×10^{-5} s^{-1} (Table S4 Supporting information). In addition, we also investigated the situation in low methane concentration conditions (the initial concentration of CH_4+HCHO and Helium (He) are 0.01 and 0.99, respectively). As shown in Fig. S9 (Supporting information), the CH_4 consumption rate has the same trend as the high concentration of CH_4 (Fig. 4). Under the temperature of 573 K and the pressure of 1 bar, the TOF of CH_4 consumption is 2.65×10^{-9} s^{-1} (Table S5 Supporting information), which is significantly lower than that on high methane concentration (2.64×10^{-5} s^{-1}), representing that the effect of reactant concentration on the production rate is significant. As shown in Figs. 4b-d, the main product of CH_4 and HCHO co-conversion is CH_3CH_2OH, which is much higher than that of C_2H_4 and H_2O, which is in agreement with the energy profiles displayed in Fig. 3a. Under the temperature of 573 K and the pressure of 1 bar, the TOF of CH_3CH_2OH production is 1.32×10^{-5} s^{-1}, which is much higher than that of C_2H_4 (4.06×10^{-18} s^{-1}) and H_2O (4.06×10^{-18} s^{-1}) (Table S4). While at the temperature of 573 K and the pressure increasing to 3 bar, CH_3CH_2OH is also the main product and the production rate increases to 1.32×10^{-4} s^{-1} (Table S4), indicative of the feasibility of this reaction under realistic conditions.

In summary, static DFT calculations and microkinetic simulations were performed to explore the one-step conversion of methane and formaldehyde to ethanol over twelve kinds of SA-FLP dual-active-site catalysts. The main conclusions are as follows. (1) The SA-FLP dual active sites can simultaneously and effectively adsorb/activate CH_4 and HCHO at SA and FLP sites, respectively. (2) Among the twelve SA-FLP catalysts, Fe_1-FLP delivers the lowest rate-determining barrier (1.15 eV), suggesting that Fe_1-FLP is the best candidate for the conversion of CH_4 and HCHO to ethanol. (3) The formation of ethanol is more facile than other products, and thus ethanol is identified as the main product of the reaction on the designed Fe_1-FLP catalysts. The TOF of CH_3CH_2OH production is 1.32×10^{-4} s^{-1} at 573 K and 3 bar. This work provides promising SA-FLP catalysts and mechanistic insights for the conversion of CH_4 and HCHO to desired C_2 chemicals.

Declaration of competing interest

The authors declare that they have no known competing financial interests or personal relationships that could have appeared to influence the work reported in this paper.

Acknowledgments

This work is supported by the National Natural Science Foundation of China (Nos. 22078257, 22038011 and 22108213), the China Postdoctoral Science Foundation (No. 2021M692548), and the Joint Fund of the Yulin University and the Dalian National Laboratory for Clean Energy (YLU-DNL Fund No. 2022001). C.-R. Chang also acknowledges the Young Talent Support Plan of Shaanxi Province. The calculations were performed by using the HPC Platform at Xi'an Jiaotong University.

Supplementary materials

Supplementary material associated with this article can be found, in the online version, at doi:10.1016/j.cclet.2023.108549.

References

[1] Y. Liu, D. Deng, X. Bao, Chem 6 (2020) 1–18.
[2] H. Cruchade, I.C. Medeiros-Costa, N. Nesterenko, et al., ACS Catal. 12 (2022) 14533–14558.
[3] P. Schwach, X. Pan, X. Bao, Chem. Rev. 117 (2017) 8497–8520.
[4] S.V.L. Mahlaba, N.H.L. Mahomed, A. Govender, et al., Angew. Chem. Int. Ed. 134 (2022) e202206841.
[5] S. Desmons, R. Fauré, S. Bontemps, ACS Catal. 9 (2019) 9575–9588.
[6] S. Zhang, M. Wang, Z. Lu, C. Ma, W. Jia, ACS Sustain. Chem. Eng. 7 (2019) 11493–11499.
[7] J. Alzeer, K.Abou Hadeed, Trends Food Sci. Technol. 58 (2016) 14–20.
[8] N.M. Eagan, M.D. Kumbhalkar, J.S. Buchanan, J.A. Dumesic, G.W. Huber, Nat. Rev. Chem. 3 (2019) 223–249.
[9] Z. Li, A.W. Lepore, M.F. Salazar, et al., Green Chem. 19 (2017) 4344–4352.
[10] Y. Jiang, W. Zhao, S. Li, et al., J. Am. Chem. Soc. 144 (2022) 15977–15987.
[11] V. Soni, V. Goel, P. Singh, A. Garg, Int. J. Chem. React. Eng. 19 (2021) 1–29.
[12] S. Zhu, J. Wang, L. Nie, ChemistrySelect 4 (2019) 12085–12098.
[13] X. Guo, G. Fang, G. Li, et al., Science 344 (2014) 616–619.

[14] Y. Liu, Z. Duan, J. Li, C. Chang, Acta Phys. Chim. Sin. 37 (2021) 2011012-0.
[15] Z. Zhu, H. Tao, J. Fu, et al., Chin. Chem. Lett. 34 (2023) 107476.
[16] C. Zhang, F. Liu, Y. Zhai, et al., Angew. Chem. Int. Ed. 51 (2012) 9628–9632.
[17] N. An, P. Wu, S. Li, M. Jia, W. Zhang, Appl. Surf. Sci. 285 (2013) 805–809.
[18] Y. Chen, J. He, H. Tian, D. Wang, Q. Yang, J. Colloid Interface Sci. 428 (2014) 1–7.
[19] J. Zhang, Y. Li, Y. Zhang, et al., Sci. Rep. 5 (2015) 12950.
[20] B.B. Chen, C. Shi, M. Crocker, Y. Wang, A.M. Zhu, Appl. Catal. B 132 (2013) 245–255.
[21] B. Bai, J. Li, ACS Catal. 4 (2014) 2753–2762.
[22] L. Ma, D. Wang, J. Li, et al., Appl. Catal. B 148-149 (2014) 36–43.
[23] Q.Y. Chang, K.Q. Wang, Z.J. Sui, et al., ACS Catal. 11 (2021) 5135–5147.
[24] J. Zhang, R.J. Zhou, Q.Y. Chang, et al., Catal. Today 368 (2021) 46–57.
[25] G. Righi, R. Magri, A. Selloni, J. Phys. Chem. C 124 (2020) 17578–17585.
[26] Y.Q. Su, I.A. Filot, J.X. Liu, E.J. Hensen, ACS Catal. 8 (2017) 75–80.
[27] Y. Zhao, C. Cui, J. Han, et al., J. Am. Chem. Soc. 138 (2016) 10191–10198.
[28] W. Zhang, M. Pu, M. Lei, Langmuir 36 (2020) 5891–5901.
[29] C. Riley, S. Zhou, D. Kunwar, et al., J. Am. Chem. Soc. 140 (2018) 12964–12973.
[30] S. Chu, X. Li, A.W. Robertson, Z. Sun, Acta Phys. Chim. Sin. 37 (2021) 2009023.
[31] C. He, R. Sun, L. Fu, et al., Chin. Chem. Lett. 33 (2022) 527–532.
[32] Y.Q. Su, Y. Wang, J.X. Liu, et al., ACS Catal. 9 (2019) 3289–3297.
[33] M. Jing, W. Song, Y. Li, et al., Chem. Eng. J. 433 (2022) 133599.
[34] P. Xie, T. Pu, A. Nie, et al., ACS Catal. 8 (2018) 4044–4048.
[35] D. Eggart, X. Huang, A. Zimina, et al., ACS Catal. (2022) 3897–3908.
[36] Y.Q. Su, J.X. Liu, I.A. Filot, L. Zhang, E.J. Hensen, ACS Catal. 8 (2018) 6552–6559.
[37] T. Ban, X.Y. Yu, H.Z. Kang, et al., J. Catal. 408 (2022) 206–215.
[38] T. Ban, X.Y. Yu, H.Z. Kang, et al., ACS Catal. 13 (2023) 1299–1309.
[39] S. Zhang, Y. Liu, M. Zhang, et al., Nat. Commun. 13 (2022) 5527.
[40] A.J. Medford, C. Shi, M.J. Hoffmann, et al., Catal. Lett. 145 (2015) 794–807.